JOURNAL OF PROPULSION AND POWER
Vol. 20, No. 1, January–February 2004

Internal Degrees of Freedom of an Actuator Disk Model

Sergei I. Chernyshenko* and Aleksei V. Privalov†
University of Southampton, Highfield, Southampton SO17 1BJ, United Kingdom

Actuator disk models can have internal degrees of freedom as, for example, in the case for models with lagged losses, governed by additional differential equations. Generally, being a system with distributed parameters, flow in the interblade passage has an infinite number of internal degrees of freedom. An attempt is made to estimate how many of them can be distinguished as the most important. The response of a blade row to time-periodic excitations is modeled by an actuator disk with internal degrees of freedom and by linearized Navier–Stokes equations, and the results are compared. It is found that in the case of subsonic flow one internal degree of freedom can be considered as the most important, both for design and off-design regimes. In the case of transonic flow in off-design regime, two internal degrees of freedom are more important than the rest. However, for the transonic design regime, no internal degrees of freedom could be distinguished as especially significant. The physical mechanisms associated with distinguished internal degrees of freedom are investigated.

Nomenclature

$\boldsymbol{E}$	=	excitation vector
F	=	actuator disk model mean square deviation function
h	=	enthalpy
$\boldsymbol{L}$, $\boldsymbol{S}$	=	vectors of actuator disk model parameters
N_{df}	=	number of degrees of freedom
N_ω	=	number of frequencies
p	=	pressure
$\boldsymbol{R}$	=	response vector
t	=	time
u, v_1	=	axial velocity
u_b, v_b, p_b, h_b	=	basic state of the unknowns
u', v', p', h'	=	perturbations of the unknowns
v, v_2	=	circumferential velocity
$\boldsymbol{v}$	=	velocity vector
δ_{ij}	=	Kronecker delta
μ	=	viscosity
ρ	=	density
τ_{ij}	=	shear stress
Ψ, M	=	matrices of actuator disk model parameters

I. Introduction

ACTUATOR disk models (ADMs) utilize the fact that the number of blades in a compressor cascade is large, whereas the pitch and the blade chord are comparable. For this reason, phenomena in a compressor can have a length scale much greater than the blade pitch and chord. Rotating stall is a good example.[1] Because of the difference in scales, the details of the flow in individual interblade passages are relatively unimportant: Large-scale phenomena react only to the bulk properties of the flow through a passage. Hence, it is possible to replace the blade row with a line or surface of discontinuity in flow parameters. This discontinuity surface is called an actuator disk. The specific relations between parameters on the opposite sides of the actuator disk constitute the model.

Various ADMs are widely used.[2–9] Our research was inspired by the impressive performance of ADMs demonstrated in the study[5] on suppressing rotating stall by active control. In the case of an incompressible flow, as in Ref. 5, ADMs give the pressure rise across and the velocity downstream from the blade row if other flow parameters on both sides of it are known. For example, in the well-known Moore[10] and Moore–Greitzer[11] model, these parameters are the velocity and its time derivative immediately upstream from the disk. The extended Moore–Greitzer model used in Ref. 5 introduces the time lags for losses so that the pressure rise depends additionally on a parameter governed by a separate differential equation. This means that the extended model has an internal degree of freedom. This internal degree of freedom can be excited by, for example, variation of the axial velocity. It would relax to the equilibrium value after the axial velocity ceases to vary. This improvement was very important for the analysis of the onset of rotating stall because without it all modes go unstable at the same critical value of the axial velocity.

In Ref. 5, a multistage compressor was considered, and internal degrees of freedom of the rotors and stators were combined into two degrees of freedom of the ADM modeling the compressor. In the present paper, we will limit our study to a single blade row.

Internal degrees of freedom can be given a more mathematical interpretation. A flow in an interblade passage is a system with distributed parameters. As such, it should normally possess an infinite number of internal degrees of freedom. In cases when the flow deviates only slightly from a steady flow, the internal degrees of freedom can be associated with the amplitudes of the eigenmodes of the linearized system of equations describing the flow in the passage. Then an ADM with one degree of freedom can be considered as an approximation in which only one major eigenmode, that is, the eigenmode having the smallest decay rate, is taken into account. An increase in the number of eigenmodes/degrees of freedom taken into account leads then to an increase in accuracy.

This interpretation gives no indication of the physical mechanisms underlying each eigenmode. In fact, there may be no such mechanisms, all eigenmodes being of the same nature and different only in scale, as in the case, for example, with eigenmodes corresponding to acoustic resonances in a fixed volume and being different mostly in wavelength only. On the other hand, some eigenmodes/degrees of freedom can have an identifiable physical mechanism. In Ref. 5, the viscous losses were considered to be involved in such a mechanism, and estimates of the corresponding timescales where made on the basis of this assumption.

The purpose of this study is to estimate whether the flow in the interblade passage has such distinguished internal degrees of freedom and if so, what their physical mechanisms are and how their number depends on the flow regime.

This problem can be addressed in several ways. It is possible to solve the eigenvalue problem for the linearized flow in the interblade passage and then try to draw conclusions from the comparative

Received 5 February 2002; revision received 17 March 2003; accepted for publication 19 March 2003.

*Professor, Aeronautics and Astronautics, School of Engineering Sciencies.

†Ph.D. Student, Aeronautics and Astronautics, School of Engineering Sciencies.

magnitudes of the decay rates of the eigenmodes. One can go even further and use the reduced-order model[12] for building the ADM and then consider the number of its internal degrees of freedom. In the present paper, a more straightforward approach is used. We anticipate that taking into account those internal degrees of freedom that have a clear physical meaning is necessary and will result in noticeable improvement in the ADM, whereas adding further degrees of freedom will give only a moderate improvement. Accordingly, our approach consists in modeling an interblade flow with an ADM and analyzing the ADM quality as a function of the number of the internal degrees of freedom it has. The ADM quality is measured by the difference between the response of a blade row and the response of the ADM modeling of this blade row to identical excitations. We then investigate the physical mechanisms associated with the internal degrees of freedom. The results obtained can yield a useful guidance on the number and nature of internal degrees of freedom that should be taken into account.

II. Navier–Stokes Model

Governing Equations

A two-dimensional compressible flow is considered. This implies that the hub-to-tip ratio is close to one and that all of the parameters are averaged in the radial direction so that only a plane flow past a row of blades need be considered. This is often assumed when ADM is used.[1,5] Taking the x axis of a Cartesian coordinate system to be parallel to the compressor axis, we then direct the y axis along the blade row, that is, in the circumferential direction. The corresponding velocity components are denoted u and v. Where convenient, we imply that $x_1 = x$, $x_2 = y$, $v_1 = u$, and $v_2 = v$ and use these notations interchangeably. Because the phenomena described with the ADM should have a length scale much greater than the blade pitch, periodicity in the direction along the blade row is imposed. This limits calculations to a single interblade passage. The unsteady perturbations are assumed to be small and are modeled using linearized equations. The exact formulation is given subsequently.

Nondimensional parameters are introduced so that $\boldsymbol{v}^* = U^*\boldsymbol{v}$, $\rho^* = \rho_0^*\rho$, $x_i^* = L^* x_i$, $p^* = [p + 1/(\gamma M_0^2)]\rho_0^* U^{*2}$, $\tau_{ij}^* = \rho_0^* U^{*2}\tau_{ij}$, $h^* = \{h + 1/[(\gamma - 1)M_0^2]\}U^{*2}$, $\mu^* = \mu_0^* F_\mu$, and $\mu_t^* = \rho_0^* U^* L^* \mu_t$. Stars mark dimensional quantities. The scales U^*, ρ_0^*, μ_0^*, and L^* correspond to a certain reference flow with the Mach number M_0. This form allows taking the limit as the Mach number tends to zero simply by substituting $M_0 = 0$ into the equations. We denote $Re = \rho_0^* U^* L/\mu_0^*$.

In Cartesian coordinates, the equations of mass, momentum, and energy conservation, respectively, take the form

$$\frac{\partial \rho}{\partial t} + \frac{\partial \rho v_i}{\partial x_i} = 0, \qquad \frac{\partial \rho v_i}{\partial t} + \frac{\partial}{\partial x_j}(\rho v_i v_j + p\delta_{ij} - \tau_{ij}) = 0$$

$$\frac{\partial}{\partial t}\left[\rho\left(\frac{h}{\gamma} + \frac{\boldsymbol{v}^2}{2} - \frac{1}{\gamma M_0^2}\right)\right] + \frac{\partial}{\partial x_j}\left[\rho v_j\left(\frac{\boldsymbol{v}^2}{2} + h\right)\right.$$

$$\left. - v^i\tau_{ij} - \left(\frac{F_\mu}{RePr_l} + \frac{\mu_t}{Pr_t}\right)\frac{\partial h}{\partial x_j}\right] = 0$$

The laminar and turbulent Prandtl numbers were taken to be $Pr_l = 0.7$ and $Pr_t = 0.9$, respectively.

The equation of state of a perfect gas takes the form

$$\rho = \frac{1 + \gamma M_0^2 p}{1 + (\gamma - 1)M_0^2 h}$$

The laminar dimensionless viscosity F_μ is given by the approximate formula

$$F_\mu = \left[1 + (\gamma - 1)M_0^2 h\right]^{\frac{3}{2}}$$

[In dimensional form this is just $\mu^*/\mu_0^* = (T/T_0)^{3/2}$.] The components τ_{ij} of the viscous stress tensor are

$$\tau_{ij} = \left(\frac{F_\mu}{Re} + \mu_t\right)E_{ij}, \qquad E_{ij} = \left(\frac{\partial v_j}{\partial x_i} + \frac{\partial v_i}{\partial x_j} - \frac{2}{3}\frac{\partial v_k}{\partial x_k}\delta_{ij}\right)$$

The turbulent viscosity μ_t is given by the generalization of the well-known Prandtl model:

$$\mu_t = l^2\Phi, \qquad \Phi = E_{ij}\frac{\partial v_i}{\partial x_j}, \qquad l = \frac{\kappa Y_1 Y_2}{(Y_1 + Y_2)}$$

The coefficient $\kappa = 0.4$, and Y_1 and Y_2 are the distances to the nearest blades. Near walls this model reduce to the Prandtl model.

For unsteady flow, $\boldsymbol{v}(t, x, y) = \boldsymbol{v}_b(x, y) + \boldsymbol{v}'(t, x, y)$, where $\boldsymbol{v}_b$ is the steady solution and $\boldsymbol{v}'$ is the perturbation. This and similar representations for other variables are then substituted in all of the equations, and only the linear terms are kept. For brevity, the linearized system is not given.

Boundary Conditions

The periodicity condition has the form $X(t, x, y + y_p) = X(t, x, y)$, where X represents the unknowns and y_p is the blade pitch. On the upstream boundary of the computational domain uniform, that is, independent of y, distributions of the velocity components and enthalpy are prescribed. On the downstream boundary, we prescribe the static pressure averaged along this boundary and the soft conditions ensuring a weak upstream effect: $\boldsymbol{v}\cdot\nabla\boldsymbol{v} = 0$ and $\boldsymbol{v}\cdot\nabla h = 0$. These conditions mean that the velocity and enthalpy derivatives along the flow direction are zero. On the surface of the blade, the no-slip condition is used, and zero heat flux is prescribed.

For the unsteady flow calculations, the velocity components and enthalpy prescribed on the left (upstream) boundary of the computational domain, u_l, v_l, and h_l, and the pressure on the right boundary p_r are functions of time.

III. ADM

General Form of the ADM

Used in combination with the inviscid flow equations, the ADM is expected to relate inviscid solutions immediately upstream and downstream from the disk representing the blade row. Near the disk, the inviscid flow can be approximated by a one-dimensional time-dependent solution of the Euler equations. In our work, the unsteady flow is described within linearized equations. As can be verified directly by substitution into the equations, one-dimensional linearized unsteady inviscid flows have the following general form:

$$\begin{aligned}
v' &= f_+(t - x/u_b)\\
u' &= g_+[t - x/(u_b + c_b)] + g_-[t - x/(u_b - c_b)]\\
h' &= h_+(t - x/u_b) + c_b g_+[t - x/(u_b + c_b)]\\
&\quad - c_b g_-[t - x/(u_b - c_b)]\\
p' &= c_b\rho_b\{g_+[t - x/(u_b + c_b)] - g_-[t - x/(u_b - c_b)]\}
\end{aligned} \tag{1}$$

where the primes denote perturbations; subscripts b denote the basic steady-state flow parameters, which are assumed to be constant; c_b is the speed of sound; and γ is the specific heat ratio. The steady state can be different on the different sides of the actuator disk. In general, the ADM gives the relation between the solutions of this form at a certain cross section upstream from the blade row at X_1, for example, and downstream from it at X_2, for example. For a given blade row and flow conditions, X_1 and X_2 are just arbitrary parameters that can be adjusted to improve the quality of the ADM.

In accord with Eq. (1), the solutions upstream and downstream from the disk can be decomposed into a sum of four waves, three of which move downstream (marked with $+$) and one moves upstream (marked with $-$). It is assumed that $c_b > u_b > 0$. As far as the ADM is concerned, it is natural to consider the waves approaching the blade row as an excitation and to consider the waves moving away from the

blade row as a response. The ADM yields the response for a given excitation. In other words, the ADM relates the Riemann invariants f_+, g_+, g_-, and h_+ on the sides of the actuator disk, or, more exactly, at a certain upstream point X_1 and a certain downstream point X_2.

Clearly, g_+, f_+, and h_+ describe perturbations moving downstream whereas g_- denotes a perturbation moving upstream. (Again, $0 < u_b < c_b$ is implied.) Therefore, the blade row subject to excitation $\boldsymbol{E}$

$$E^1 = g_+|_{X_1}, \qquad E^2 = f_+|_{X_1}$$
$$E^3 = g_-|_{X_2}, \qquad E^4 = h_+|_{X_1} \tag{2}$$

produces the response

$$R^1 = g_+|_{X_2}, \qquad R^2 = f_+|_{X_2}$$
$$R^3 = g_-|_{X_1}, \qquad R^4 = h_+|_{X_2} \tag{3}$$

The ADM studied in the present paper relates $\boldsymbol{R}$ to $\boldsymbol{E}$ with

$$R^j = \Psi^{j\cdot}_{\cdot i} E^i + M^{j\cdot}_{\cdot i} \frac{\mathrm{d}E^i}{\mathrm{d}t} - \sum_{k=1}^{N_{\mathrm{df}}} \boldsymbol{L}^{j\cdot}_{\cdot k} s^k \tag{4}$$

and specifies that

$$\sigma_k \frac{\mathrm{d}s_k}{\mathrm{d}t} = \boldsymbol{S}_{ik} E^i - s_k, \qquad k = 1, \ldots, N_{\mathrm{df}} \tag{5}$$

where N_{df} is the number of internal degrees of freedom of the actuator disk and s_k are the amplitudes of the excited internal modes. It is quite possible that $N_{\mathrm{df}} = 0$, but generally we expect it to be 1 or 2.

This specific form of ADM is, in fact, a simple generalization of the extended Moore[10] and Moore–Greitzer[11] model successfully used in Ref.5, where $\boldsymbol{R}$ and $\boldsymbol{E}$ were scalars, the total to static pressure rise and the axial velocity, respectively, and s_1 and s_2 were the losses in stators and rotors.

Matrices $(\Psi^{j\cdot}_{\cdot i})$, $(M^{j\cdot}_{\cdot i})$, an integer value N_{df}, vectors $\boldsymbol{L}^{j\cdot}_{\cdot k}$ and $\boldsymbol{S}_{ik}$, time lag coefficients σ_k, $k = 1, \ldots, N_{\mathrm{df}}$, and edges X_1 and X_2 are the parameters of the actuator disk model. They should be chosen to fit better the behavior of the real blade row.

Fitting ADM to the Blade Row and Estimating Its Quality

To determine the ADM parameters and to estimate its quality, the response of the blade row to time-periodic excitation can be used. For perturbations proportional to $e^{i\omega t}$, taking the time derivative is equivalent to multiplication by $i\omega$. Then

$$R^j = A^j_i(\omega) E^i \tag{6}$$

where

$$A^j_i(\omega) = \Psi^{j\cdot}_{\cdot i} + i\omega M^{j\cdot}_{\cdot i} - \sum_{k=1}^{N_{\mathrm{df}}} \frac{\boldsymbol{L}^{j\cdot}_{\cdot k} \boldsymbol{S}_{ik}}{1 + i\omega\sigma_k}$$

This gives the relation between the Riemann invariants at X_1 and X_2. In the case of a time-periodic excitation, the Riemann invariants can be represented in the form

$$f_+ = V_+ \exp[i\omega(t - x)/u_b]$$
$$g_+ = U_+ \exp\{i\omega[(t - x)/(c_b + u_b)]\}$$
$$g_- = U_- \exp\{i\omega[(t + x)/(c_b - u_b)]\}$$
$$h_+ = H_+ \exp[i\omega(t - x)/u_b] \tag{7}$$

where V_+, U_+, U_-, and H_+ do not depend on t or x (except that they, as well as u_b and c_b, are different on the different sides of the actuator disk).

When Eqs. (1) and (7) are used, it is possible to express u', v', p', and h' via V_+, U_+, U_-, and H_+ and vice versa. If the perturbations u', v', p', and h' are calculated numerically using the linearized Navier–Stokes equations, it is also possible to recalculate V_+, U_+, U_-, and H_+ with the same formulas. In general, these quantities will not be constant because the Navier–Stokes solution is not one dimensional and it is not inviscid. However, in accordance with the idea of the ADM approach, we expect that far from the blades the variations in circumferential direction and the viscosity effects should be small. Then V_+, U_+, U_-, and H_+ should be approximately constant in the far field. If this is the case, then four linear-independent linearized Navier–Stokes solutions provide enough information for calculating the matrix $A^j_{i\,\mathrm{calc}}(\omega)$ such that taking

$$R^j = A^j_{i\,\mathrm{calc}}(\omega) E^i \tag{8}$$

and using the one-dimensional inviscid solutions for calculating the flow parameters at other x will reproduce the linearized Navier–Stokes results in the far field. Then

$$F = \sqrt{\frac{1}{\omega_{\max}} \int_0^{\omega_{\max}} \sum_{i,j} \left| A^j_{i\,\mathrm{calc}}(\omega) - A^j_i(\omega) \right|^2 \mathrm{d}\omega} \tag{9}$$

estimates the quality of the ADM. For a given N_{df}, minimizing F by varying all other parameters of the ADM gives the ADM for the specific blade row. The minimum value $F_{\min}(N_{\mathrm{df}})$ as a function of the number of internal degrees of freedom N_{df} will be the object of our analysis.

IV. Numerical Implementation

In many respects our numerical approach is fairly standard. The grid used is shown in Fig. 1. Spatial discretization of second-order accuracy was applied, with convective terms approximated using third-order upstream differences, following Leonard.[13] The scheme was strictly conservative. For validation purposes an arbitrary body force represented by a subroutine was introduced into the Navier–Stokes equations. Substituting an arbitrary velocity distribution given by an explicit expression into the Navier–Stokes equations gives explicitly the body force for which this velocity distribution is an exact solution. This body force was then programmed into the code, and the numerical solution found was compared with the exact solution. In this way, the program was tested against quite complicated velocity distributions. The call to the body-force subroutine was then commented out. The results were also checked by refining the grid.

Several features of our numerical approach deserve more detailed discussion. The steady solution of the Navier–Stokes equations was calculated by the Newton method. This has two important advantages. First, time-marching schemes cannot be used when the steady state is unstable. Other simple iteration methods are also known to inherit some of the physical instability of the flow. Because of that, calculations of separated flows, which, for example, are of interest for rotating stall applications of ADM, can be difficult. In contrast, the Newton method is guaranteed to converge provided that

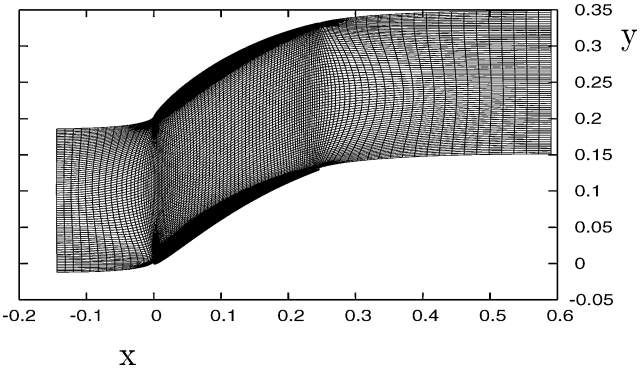

Fig. 1 Grid and calculation domain.

the initial approximation is sufficiently close to the solution. This can be achieved by calculating the solution for, for example, a small Reynolds number Re and then stepping in the Reynolds number, using the solution from the previous step as the initial approximation. The high efficiency of the Newton method for calculating separated flows at high Reynolds numbers was demonstrated earlier. In fact, the so far most advanced calculations of steady laminar separated flows at high values of Reynolds number[14] were performed using the Newton method.

Second, use of the Newton method for calculating the steady flow has additional advantages for calculating the linearized time periodic flow. In the Newton method, each iteration consists in solving the linearized system. In our code the matrix of this linearized system is obtained by numerical differentiation of the functions representing the nonlinear algebraic equations. Note that the matrix of the unsteady linearized system can easily be obtained from the matrix of the steady linearized system. After spatial discretization, the (nonlinear) unsteady equations can be written as

$$\frac{\partial \boldsymbol{N}}{\partial \boldsymbol{W}}\frac{\mathrm{d}\boldsymbol{W}}{\mathrm{d}t} + \boldsymbol{G}(\boldsymbol{W}, \boldsymbol{B}) = 0$$

where $\boldsymbol{W}$ is a vector of the unknowns, whose components are the values of u, v, p, etc., at the corresponding grid nodes. Vector $\boldsymbol{B}$ is the vector of boundary conditions, in particular, in the case in question, its components are velocity components U, V, and enthalpy H far upstream and pressure P downstream, so that the boundary conditions for velocity far upstream, for example, are $u_{|\text{far upstream}} = U(t)$. The vector function $\boldsymbol{N}(\boldsymbol{W})$ has a relatively simple form, for example, its components corresponding to the continuity equation are just $\rho(p, h)$ with p and h taken at the corresponding node.

Steady flow satisfies the system

$$\boldsymbol{G}(\boldsymbol{W}, \boldsymbol{B}) = 0 \tag{10}$$

with $\boldsymbol{B} = \text{const}$. When solving this system with Newton's method, one solves the equation $(\partial \boldsymbol{G}/\partial \boldsymbol{W})\Delta \boldsymbol{W} + \boldsymbol{G}(\boldsymbol{W}_n, \boldsymbol{B}) = 0$ and iterates as $\boldsymbol{W}_{n+1} = \boldsymbol{W}_n + \Delta \boldsymbol{W}$. Now, we assume that unsteady perturbations are small and periodic, so that $\boldsymbol{W} = \boldsymbol{W}_b + \boldsymbol{Z}e^{i\omega t}$ and $\boldsymbol{B} = \boldsymbol{B}_b + \boldsymbol{A}e^{i\omega t}$ with $\boldsymbol{A}$ given. Substituting this into the unsteady equations gives

$$\left(i\omega\frac{\partial \boldsymbol{N}}{\partial \boldsymbol{W}} + \frac{\partial \boldsymbol{G}}{\partial \boldsymbol{W}}\right)\boldsymbol{Z} + \frac{\partial \boldsymbol{G}}{\partial \boldsymbol{B}}\boldsymbol{E} = 0$$

We modify the steady solver first in such a way that instead of solving Eq. (10) it solves $i\omega \boldsymbol{N}(\boldsymbol{W}) + \boldsymbol{G}(\boldsymbol{W}, \boldsymbol{B}) = 0$. This does not makes sense in itself except when $\omega = 0$. However, the modification is simple because, in the code, the equations are described by a subroutine calculating $\boldsymbol{G}(\boldsymbol{W}, \boldsymbol{B})$, with the matrix of derivatives $\partial \boldsymbol{G}/\partial \boldsymbol{W}$ being calculated using numerical differentiation. Adding $i\omega \boldsymbol{N}(\boldsymbol{W})$ to $\boldsymbol{G}(\boldsymbol{W}, \boldsymbol{B})$ in this subroutine is simple because $\boldsymbol{N}(\boldsymbol{W})$ is simple and does not contain spatial derivatives. Note that the matrix of derivatives calculated by this modified code is the same as the matrix needed for linearized unsteady calculations. Moreover, the matrix $\partial \boldsymbol{G}/\partial \boldsymbol{B}$, which is also needed, can also be calculated by numerical differentiation. As a result, the majority of the subroutines of the steady solver are utilized in the unsteady solver. In this way, any modification in the steady code, for example, a change in the turbulence model, is automatically taken into account in the unsteady code.

The general procedure for the computations was as follows. First, for a given Mach number and the boundary conditions, the steady solution was calculated, and the entire flowfield stored. Then, for a set of frequencies ω, the unsteady code was used to calculate the response of the blade row to four independent excitations of the form

$$u = u_b(\text{upstream}) + E_1 e^{i\omega t}, \qquad v = v_b(\text{upstream}) + E_2 e^{i\omega t}$$

$$p = p_b(\text{downstream}) + E_3 e^{i\omega t}, \qquad h = h_b(\text{upstream}) + E_4 e^{i\omega t} \tag{11}$$

at the upstream and downstream boundaries of the calculation domain, respectively, with $\boldsymbol{E} = (1, 0, 0, 0)$, $\boldsymbol{E} = (0, 1, 0, 0)$, $\boldsymbol{E} = (0, 0, 1, 0)$, and $\boldsymbol{E} = (0, 0, 0, 1)$. This gives the four independent solutions needed for calculating $A^j_{i\,\text{calc}}(\omega)$ in Eq. (8). For each of these solutions, V_+, U_+, U_-, and H_+ were calculated and averaged in the circumferential direction. Their dependence on x was analyzed visually, and the approximately constant values upstream and downstream from the blade row were used for calculating $A^j_{i\,\text{calc}}(\omega)$.

Calculation results for different ω were written to the disk and used by a separate code for calculating the ADM parameters minimizing the function F [given by the discrete version of Eq. (9)]. The minimization is performed in two steps. For X_1, X_2, σ_k, and $\boldsymbol{L}^{j\cdot}_{k}$ fixed, the minimization with respect to all other parameters is just a least-squares problem. This leaves F as a function of X_1, X_2, σ_k, and $L^{j\cdot}_{k}$. To minimize this function, the modified APPSPACK freeware calculation package was used.

V. Results and Discussion

Setup

Calculations were performed for a cascade of NACA65 airfoils of nondimensional chord length 0.3. The stagger angle was 35 deg and the pitch was 0.2. The calculation domain and the grid are shown in Fig. 1. A grid of 114×78 nodes was found to be sufficient to obtain grid independent results. The circumferential velocity far upstream was equal to 1, in other words, its dimensional value was used as the velocity scale and also for calculating the Reynolds Re and the Mach M_0 numbers. All calculations were performed for $Re = 10^4$. Calculations were performed for $M_0 = 0.4$ and for $M_0 = 1$. In the steady flow calculations, the axial velocity was varied. The nondimensional enthalpy h far upstream and the nondimensional pressure p far downstream were taken to be zero. (Note how these nondimensional quantities were introduced in Sec. II). For unsteady calculations, the boundary conditions were perturbed according to Eq. (11). The case $M_0 = 0.4$ corresponds to almost incompressible flow. For $M_0 = 1$, the flow upstream from the cascade was supersonic with the Mach number M close to unity. For example, for the upstream axial velocity equal to 0.55 (as in one of our special test cases), $M = \sqrt{(1 + 0.55^2)} = 1.145$. The pressure isolines for flows with $M_0 = 1$ showed a weak shock (or, rather, a compression wave) forming inside the interblade passage, and the entire flow was in fact transonic.

Steady Flow Solutions

Figure 2 shows the total-to-static pressure rise ψ (the static pressure downstream minus the total pressure upstream) as a function of the axial velocity far upstream u_∞ for $M_0 = 0.4$. Figure 2 also shows

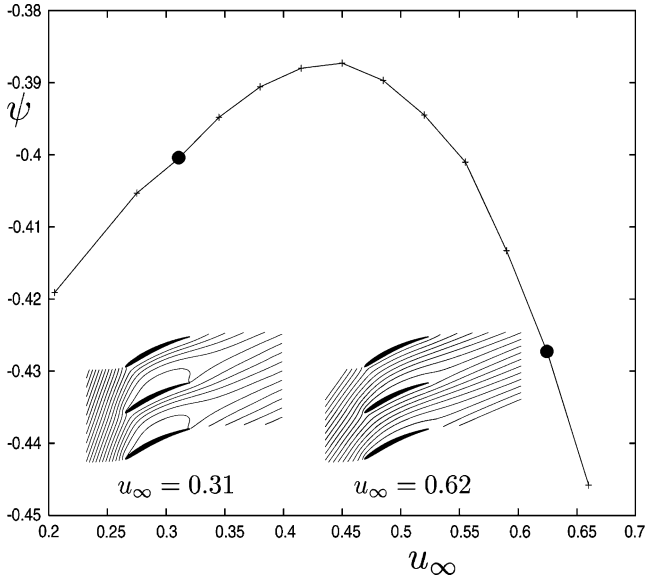

Fig. 2 Total-to-static pressure rise and the flow patterns.

the flow streamlines for two values of u_∞, with massive separation in one case. According to Longley,[1] rotating stall can be expected when $\partial\psi/\partial u_\infty > 0$. The result demonstrates that the Newton method can be used to calculate steady but physically unstable flows, in particular, in that range of u_∞, which is of interest for the rotating stall stability analysis.

Similar calculations were also performed for $M_0 = 1$. Both for $M_0 = 0.4$ and $M_0 = 1$, the separation was absent or insignificant for $u_\infty = 0.55$, and it was well pronounced for $u_\infty = 0.45$. These two values of u_∞ were selected to represent the design and off-design regimes, respectively, each for subsonic ($M_0 = 0.4$) and transonic ($M_0 = 1$) flow, in further unsteady calculations.

Unsteady Calculations

The unsteady calculations were performed for $\omega = (0, 0.2, \ldots, 3.8)$ in each of the four basic steady states, that is, for the subsonic design and off-design and transonic design and off-design states. For a sinusoidal perturbation wave running along the blade row with velocity V, the wavelength is $\lambda = 2\pi V/\omega$. For $V = 0.5$ and $\omega = 3.8$, this gives the wavelength about four times the blade pitch in our calculations. Higher frequencies would correspond to shorter wavelength, in which case an ADM is not expected to be used anyway. With Eq. (9), 10 values of ω proved to be sufficient for calculating the minimum of F, which did not change considerably when fewer points in ω range were used. In the present paper, F was calculated by the first-order-accurate discrete version of Eq. (9):

$$F = \sqrt{\sum_{ijl} \left| A^j_{i\,\mathrm{calc}}(\omega_l) - A^j_i(\omega_l) \right|^2 \Big/ N_\omega} \qquad (12)$$

The primary goal of the unsteady flow calculations is to determine $A^j_{i\,\mathrm{calc}}(\omega)$ in Eq. (8). For this, constant values of V_+, U_+, U_-, and H_+ should be determined in the far field upstream and downstream of the blade row. Generally, the unsteady flow is not uniform. This nonuniformity slowly decreases as the distance from the blades increases, as can be seen, for example, in Fig. 3. This shows the perturbation of the axial velocity at $t = 0$ in the design case ($M = 1.0$) for $\omega = 3.8$, when the axial velocity upstream is excited (as $\cos \omega t$).

Whereas the flow parameters are far from uniform, V_+, U_-, U_+, and H_+ averaged in the circumferential direction become independent of the axial coordinate remarkably close to the blades. This is clearly indicated by the flat portions of all of the curves (in Fig. 4). Near the downstream boundary of the calculation domain, there is a certain variation. The reason is that the boundary conditions are not nonreflecting. However, it is sufficient to use V_+, U_-, U_+, and H_+ from the flat portions of the curves. Similar results were obtained for all 80 solutions. Two cross sections were chosen on each flat portion, namely, at $x = -0.1$ and $x = 0.5$, and the values of V_+, U_-, U_+, and H_+ at these points were used for determining $A^j_{i\,\mathrm{calc}}(\omega)$. Figure 4 may seem to suggest that, because the one-dimensional

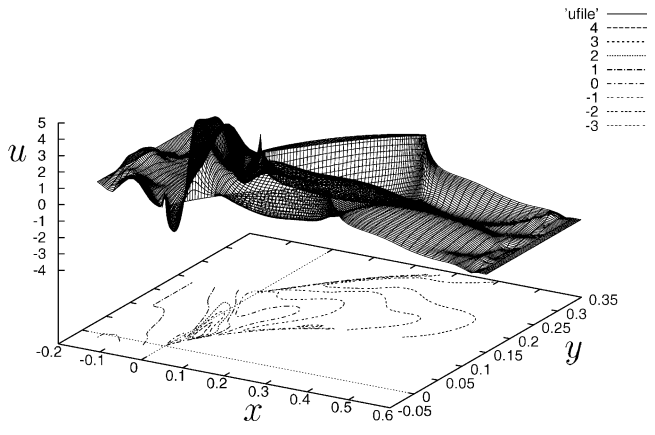

Fig. 3 Axial velocity perturbation; off-design case: $M = 1$, $u_{\mathrm{uptream}} = 0.45$, and $\omega = 3.8$.

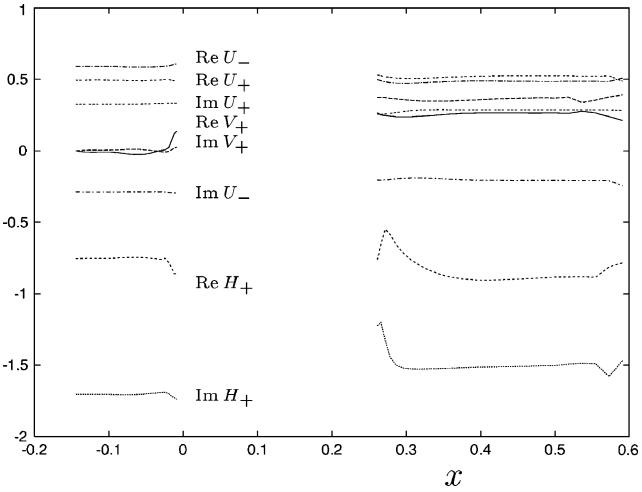

Fig. 4 Typical behavior of amplitudes of Riemann invariants averaged in circumferential direction.

averaged description applies well near the blades, it may be possible to calculate the bulk properties of a compressor stage consisting of a rotor and a stator as a simple stack of the rotor and stator ADMs obtained for each of them separately. However, one should take into account that the downstream blade row located close to the upstream blade row will be subject to the vortex perturbations of the base flow due to the viscous wakes. This effect is not present in our calculations. In fact, the interaction of the viscous wakes with our downstream boundary conditions causes the deviation from the quasi-one-dimensional behavior observed near the downstream boundary of the calculation domain in Fig. 4, thus, indicating that the rotor–stator interactions may be important.

ADM Results

The results of the unsteady calculations were used to find the best ADM. In each of the test cases four ADMs, for $N_{\mathrm{df}} = 0$, $N_{\mathrm{df}} = 1$, $N_{\mathrm{df}} = 2$, and $N_{\mathrm{df}} = 3$ were built. The minimum of the mean square deviation function F [see Eq. (9)] attained gives a quantitative characteristic of the overall performance of the ADM. This characteristic is, however, rather abstract. More physical insight into the ADM performance can be obtained by direct comparisons of the predictions for the same flow obtained with the Navier–Stokes code and the ADM. To circumvent the difficulty associated with the reflective boundary conditions causing nonuniformity near the boundaries of the calculation domain, we perform the comparison for a somewhat shorter region only. This effectively means that, using V_+, U_-, U_+, and H_+ from the flat portions in Fig. 4, we recalculate the corresponding flow parameters and then feed their values at the downstream and upstream boundaries as an input to a simple code calculating the flow using the ADM. Figures 5 and 6 show the typical results of such a comparison. Similar levels of agreement were obtained for other values of ω and in different regimes. This comparison also validates the minimization procedure. Note the number of degrees of freedom given in the upper left corner of Figs. 5 and 6. From Figs. 5 and 6, it is clear that introducing internal degrees of freedom improves the ADM and that two degrees of freedom give quite reasonable accuracy. Note that enthalpy turns out to be most difficult to model with ADM. This can be compared with H_+ having the most pronounced variation in Fig. 4. However, further analysis of this is outside the scope of the present paper.

Let us consider now the minimum of the mean square deviation F as a function of the number of internal degrees of freedom N_{df}. We anticipate a sudden improvement in the ADM quality as the number of the internal degrees of freedom of the ADM becomes equal to the number of distinguished degrees of freedom of the flow in the interblade passage. Figures 7 and 8 show $\log(\min F)$ vs N_{df} for design and off-design regimes, respectively. The anticipated behavior is observed in three of four cases. For both design and off-design subsonic flow, introducing the first internal degree of freedom gives

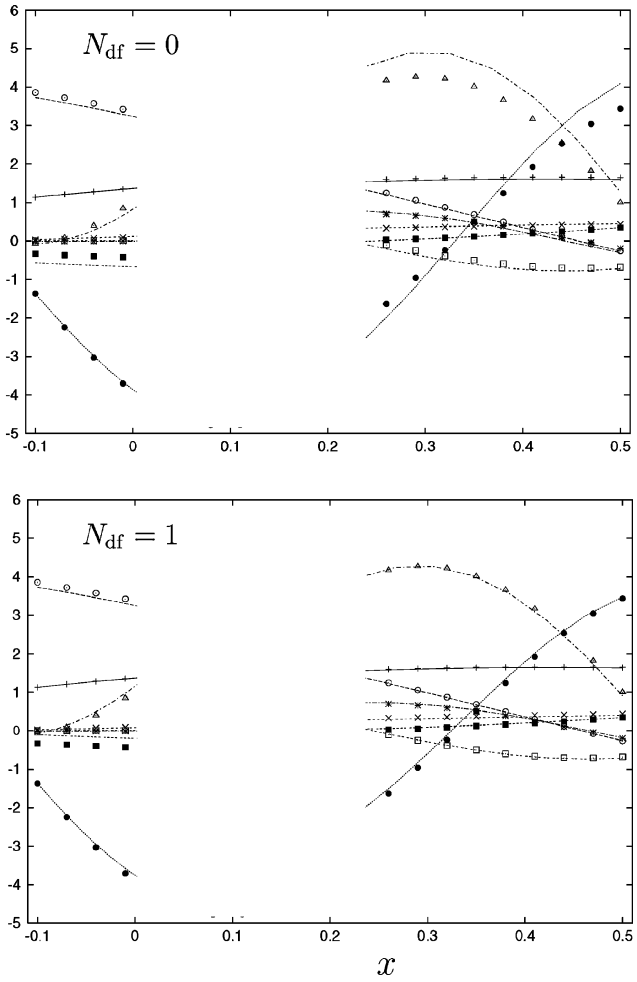

Fig. 5 Comparison results, subsonic design case, $E = (1, 0, 0, 0)$, $\omega = 3.8$: +, *Re u′*; ×, *Im u′*; ∗, *Re v′*; □, *Im v′*; ■, *Re p′*; ○, *Im p′*; ●, *Re h′*; △, *Im h′*; points, recalculated from V_+, U_-, U_+, and H_+; and curves, obtained with ADM.

much greater effect than increasing N_{df} further. This corresponds to only one essential degree of freedom. In the transonic off-design regime, such sharp improvement happens when N_{df} changes from one to two, thus, corresponding to two essential degrees of freedom. However, for the transonic design regime, there is no such sudden improvement. Instead, adding one degree of freedom reduces the log(min F) by almost the same value for $N_{df} = 0$, 1, and 2. Note that min F decreases quickly as N_{df} increases in all cases. Therefore, for practical purposes, N_{df} can indeed be assumed to be quite small. The results obtained indicate also that, when compressibility effects are important, higher values of N_{df} are needed.

Physical Mechanisms

With $N_{df} = 0$, the ADM (4) gives the response as a function of the instantaneous values of the excitation and its time derivative. If a similar assumption is made about the linearized Navier–Stokes solutions, then for, for example, the flow excited by variation of the upstream enthalpy $h'_l(t)$, one obtains for u'

$$u'(t, x, y) = G(x, y)h'_l(t) + H(x, y)\frac{\mathrm{d}h'_l}{\mathrm{d}t}(t) \qquad (13)$$

Our calculations were performed for $h'_l = \exp i\omega t$, so that $u'(t, x, y) = u'_\omega(x, y)\exp i\omega t$. Therefore, $u'_\omega(x, y) = G(x, y) + i\omega H(x, y)$. Because $G(x, y)$ and $H(x, y)$ are real valued and independent of ω, for any two values ω_1 and ω_2

$$D(x, y) = Re\left(u'_{\omega_1} - u'_{\omega_2}\right) + iIm\left[(\omega_2/\omega_1)u'_{\omega_1} - u'_{\omega_2}\right] = 0$$

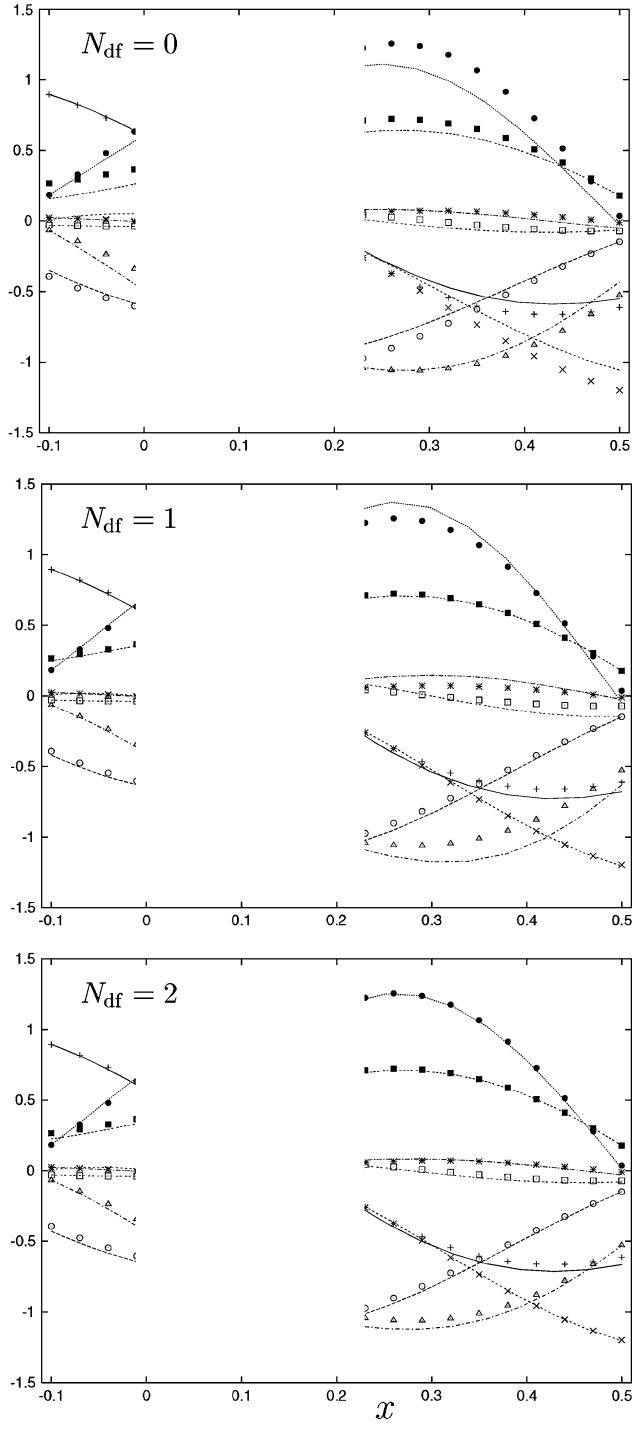

Fig. 6 Same as Fig. 5, but for the transonic off-design case.

Note that due to its instantaneous nature Eq. (13) cannot describe a wave propagating with a finite speed. In contrast, the inviscid equations upstream and downstream from the actuator, which are used in combination with ADM, do describe such waves. Therefore, those deviations of $D(x, y)$ from zero that have the form of a propagating wave do not necessarily invalidate the assumption $N_{df} = 0$. Because inside the interblade passage the wave path is not straight, the wave takes more time to pass through than if it were propagating in the absence of blades. In the ADM (4), this effect and the difference in the propagation speed upstream and downstream from the blades can be compensated by adjusting the edges X_1 and X_2 of the actuator. However, this is not enough when there are two waves propagating with different speeds. Ideally, the blade row response should be related to the excitation by an equation with delayed argument, the delay being equal to the wave passing time.

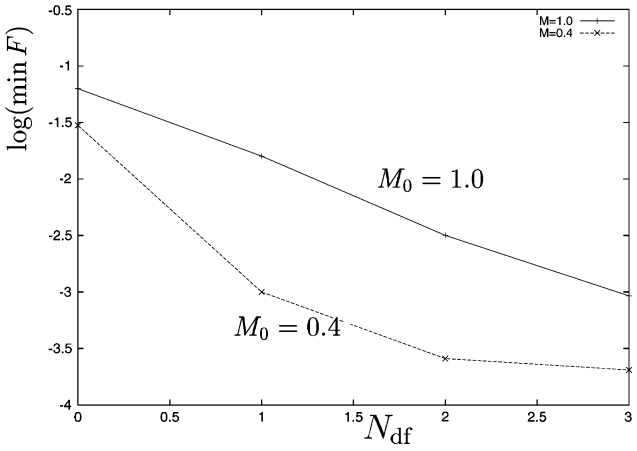

Fig. 7 Mean square deviation F between ADM and Navier–Stokes results, design case; note the logarithm.

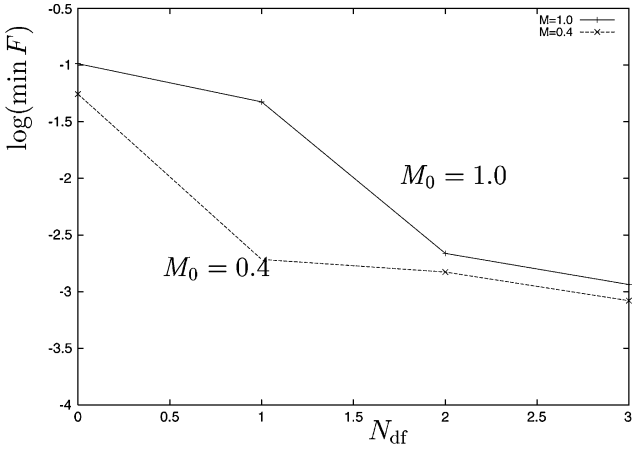

Fig. 8 Mean square deviation F between ADM and Navier–Stokes results, off-design case.

If the passing time is small as compared to the characteristic time of the process in the compressor, internal degrees of freedom approximate the relationship with a delayed argument, with accuracy gradually increasing with N_{df}. Of course, these internal degrees of freedom cannot be interpreted physically. This appears to be the case for the transonic design regime in Fig. 7. Quite naturally, propagating almost sinusoidal waves are present in the majority of our solutions. They occupy the entire calculation domain and are distorted only near the blades. For time-periodic flows, the propagation speed is related to the wavelength. In subsonic flows, we observe only a single wavelength, whereas in transonic flows there are two. It is natural to assume that one wavelength corresponds to vorticity and entropy waves, propagating downstream with the average axial flow velocity, whereas the other corresponds to sound waves propagating upstream with speed equal to the difference between the speed of sound and the mean flow velocity. The sound waves moving downstream pass quickly through the calculation domain and are not observed at all, and the upstream moving sound waves are observed only in transonic cases.

Those deviations of $D(x, y)$ from zero that do not have the form of a global wave can be expected to correspond to internal degrees of freedom having physical meaning. A complex-valued quantity such as $D(x, y)$ can be introduced for each of the four variables u', v', p', and h' in each of the four time-dependent solutions we calculated in each of the four regimes. If represented as isolines or surfaces, this amounts to 128 pictures. With the additional complication of global waves being present in the pictures, such a volume of data is difficult to analyze. We developed an interactive animation system showing the surface and isolines of $D(x, y)\exp(2\pi i\tau)$, where τ is artificial time. The resulting on-screen picture is similar to Fig. 3, but the surface is moving. The shapes of the surface of $D(x, y)\exp(2\pi i\tau)$ are usually less complicated than Fig. 3, because the part of the solutions that can be represented in the form of Eq. (13) does not manifest itself. This simplification is the purpose of introducing $D(x, y)$. Animation helps to distinguish important features even against the background of propagating global waves. The variable and solution on display, and the picture orientation, ranges and isoline contour levels can be changed interactively. The system consists of a standard Unix/Linux command-driven graphic tool, gnuplot, receiving commands through a named pipe, and a FORTRAN code generating the commands and directing them into that pipe. A link to a simple example of such gnuplot/FORTRAN animation is given in the web page of Chernyshenko accessible from the Aerodynamics and Flight Mechanics Research Group website (http://www.afm.ses.soton.ac.uk). The FORTRAN code interacts with the user by periodically reading a data file whose contents can be changed with any editing tool.

Values $\omega_1 = 0.2$ and $\omega_2 = 3.8$ were used. Three processes of interest were identified by observing the animations and are illustrated. Figure 9 shows a succession of the positions of the region in which $0 < h' < 0.05$ at $\tau = 0.1, 0.3, 0.5, \ldots$, for the subsonic design regime. The perturbation was excited by varying the enthalpy far upstream [$\boldsymbol{E} = (0, 0, 0, 1)$, see Eq. (11)]. As expected, in essence the enthalpy wave is just advected downstream at the flow velocity. Because of the no-slip condition near the wall, the initially flat wave becomes curved. Accordingly, different parts of the wave reach the exit of the interblade passage at different times. Such nonuniformity in the passing time was observed in all regimes. This wave distortion cannot be described by a single internal degree of freedom. Therefore, it should lead to only a gradual increase in ADM quality as N_{df} increases.

In off-design cases, animations showed an intensive activity inside the separation eddy. In Fig. 10, the steady streamline pattern is compared with the shape of the region (shown with thick dashed curve) where $D_h > 1.4$ at $\tau = 0.425$ for $\boldsymbol{E} = (0, 0, 0, 1)$, where D_h

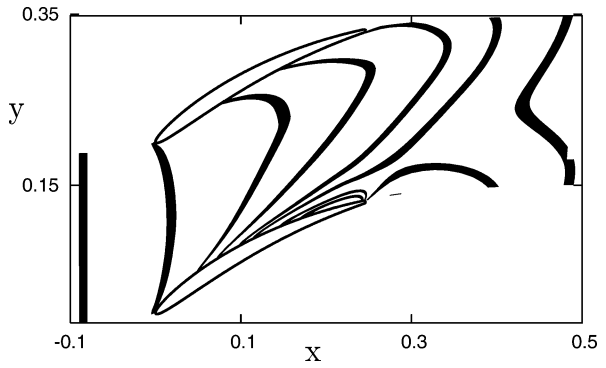

Fig. 9 Wave distortion mechanism.

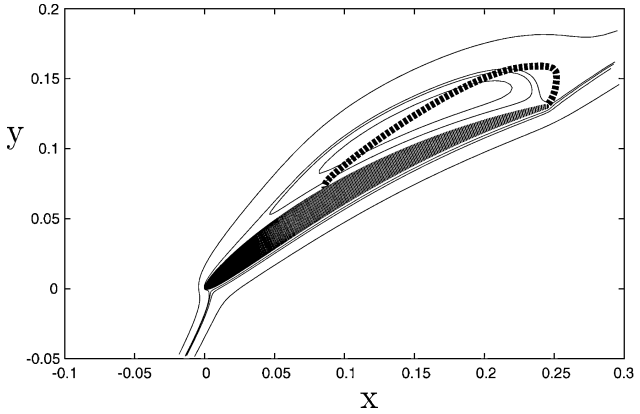

Fig. 10 Separation mechanism, dashed curve shows the region of high deviation from no inernal-degrees-of-freedom behavior.

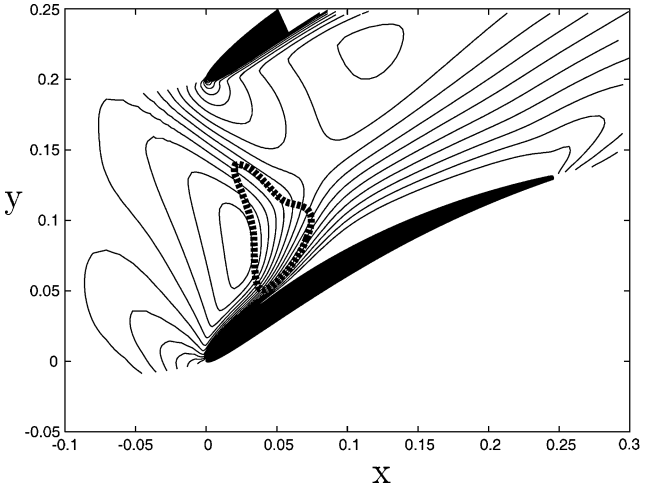

Fig. 11 Viscous–inviscid interaction mechanism.

denotes $D(x, y)$ constructed from h'. Note that isolines of D_h at other τ can exhibit a quite different pattern, but animations clearly indicate that the inside of the eddy lives its own life, behaving independently. This is the case when indeed a single degree of freedom, expressed, for example, as the amount of vorticity in the eddy, can be expected to give a significant contribution to ADM quality.

In transonic cases, a region of relatively high Mach number exists in the steady flow. Figure 11 shows the isolines of M for steady flow in the transonic design case and the location and shape of another region of high activity identified from animations [$D_h > 1.2, \tau = 0.95$, $\boldsymbol{E} = (0, 0, 0, 1)$]. In this case, the high-activity region overlaps the boundary layer and the supersonic flow region upstream from the shock/compression wave, in other words, it overlaps the region of viscous–inviscid interaction.[15] The dimensions of the viscous–inviscid interaction region are relatively small. For this reason its deviation from equilibrium state can quite likely be modeled with a single degree of freedom, at least as far as the bulk ADM response is concerned.

The emerging pattern seems to be consistent. We identified two mechanisms, namely, global waves propagating with two different speeds and distortion of a propagating wave, that cannot be expected to correspond to single internal degrees of freedom and two mechanisms, involving separation and viscous–inviscid boundary-layer–shock-wave interaction that are more likely to correspond to distinguished internal degrees of freedom. In the subsonic design regime, only one of the first mechanisms, the wave distortion, is present. Accordingly, the convergence (as N_{df} increases) is the fastest, but there is no sudden improvement in the ADM with N_{df} increased by one. In the supersonic design regime, both the first two mechanisms are present, and accordingly, the convergence is slower. The viscous–inviscid interaction is also present in this case; however, no sharp improvements in ADM are observed. Indeed, the very nature of the viscous–inviscid interaction is such that, when it does not precede the boundary-layer separation, its overall effect is small. However, if the boundary layer separates, as in the off-design transonic case, then viscous–inviscid interaction becomes much more important, and two degrees of freedom are needed to model it and the separation region itself. This explains the sudden improvement in ADM when two degrees of freedom are taken into account (Fig. 8). In the subsonic off-design case, the separation corresponds to only one distinguished internal degree of freedom.

These results have important implications for designing an ADM. First, depending on the flow regime, the results obtained may suggest the number of internal degrees of freedom to be taken into account. Second, the two-wave-speed mechanism, present in the transonic case, can obviously be better modeled by relating the response to the excitation by an equation with delayed argument, and such an ADM can probably be proposed. However, solving the Euler equations in combination with an ADM involving relationships with delayed arguments can be more difficult. The wave-distortion mechanism hardly can be accurately modeled with any ADM, and if and when it is of major importance, other ways of compressor modeling may be preferable.

VI. Conclusions

1) The Newton method is applicable for calculating steady mean turbulent compressible flow in a compressor, even in regimes when physical instability is quite strong. This includes the case when the compressor characteristics have a positive slope and/or there is a massive separation.

2) The use of the Newton method for solving the steady problem conveniently combines with solving the linearized unsteady problem.

3) It was found that upstream and downstream from the blade row averaged Riemann invariants exhibit quasi-one-dimensional behavior not only far from the blades but also remarkably close to them. This allows one to use relatively short computational domains.

4) In all cases, an ADM with two internal degrees of freedom was found to give quite accurate descriptions of the behavior of a compressor blade row in terms of upstream and downstream flow parameters averaged in the circumferential direction.

5) Four mechanisms were identified as responsible for the deviation of the blade row response from the response given by the ADM without internal degrees of freedom: a) difference in propagation speed for waves of different nature (present in transonic flows and poorly modeled with internal degrees of freedom), b) wave distortion (present always, poorly modeled with internal degrees of freedom), c) separation (present in the off-design regimes, well modeled with an internal degree of freedom), and d) viscous–inviscid interaction (present in transonic regime, well modeled with internal degree of freedom but essential only in the off-design regime).

Acknowledgments

This research was supported in part by the Russian Foundation for Basic Research, project 96-01-01291 and by the Engineering and Physical Sciences Research Council, United Kingdom, Grant GR/L58835 (with a contribution from Rolls-Royce plc). A. Privalov acknowledges support from the School of Engineering Sciences, University of Southampton and U.K. Scholarships for International Research Students via studentships. The authors are grateful to A. I. Ruban and P. W. Duck for valuable discussions at early stages of this research, I. P. Castro for help with the text, and to the referees for the encouragement and advice that resulted in considerable improvement of the revised paper.

References

[1]Longley, J. P., "A Review of Nonsteady Flow Models for Compressor Stability," *Journal of Turbomachinery*, Vol. 116, April 1994, pp. 202–215.

[2]Ehrich, F. F., Spakovszky, Z. S., Martinez-Sanchez, M., Song, S. J., Wisler, D. C., Storace, A. F., Shin, H.-W., and Beacher, B. F., "Unsteady Flow and Whirl-Inducing Forces in Axial-Flow Compressors: Part II—Analysis," *Journal of Turbomachinery*, Vol. 123, No. 3, July 2001, pp. 446–452.

[3]Micklow, J., and Jeffers, J., "Semi-actuator Disk Theory for Compressor Choke Flutter," NASA Contractor Reports NASA-CR-3426, June 1981.

[4]Billet, G., Laval, P., and Chevalier, P., "Response of an Axial Compressor to a Distorted Inlet Flow," *I Mech E Conference Publications*, Inst. of Mechanical Engineers, Birmingham, England, U.K., 1984, pp. 211–220.

[5]Haynes, J. M., Hendricks, G. J., and Epstein, A. H., "Active Stabilization of Rotating Stall in a Three-Stage Axial Compressor," *Journal of Turbomachinery*, Vol. 116, April 1994, pp. 226–239.

[6]Xiao, M., and Basar, T., "Analysis and Control of Multi-mode Moore-Greitzer Compressor Models," *Proceedings of the American Control Conference*, San Diego, CA, Vol. 4, 1999, pp. 2647–2651.

[7]Aernouts, W., Roose, D., and Sepulchre, R.,"Delayed Control of a Moore–Greitzer Axial Compressor Model," *International Journal of Bifurcation and Chaos*, Vol. 10, May 2000, pp. 1157–1164.

[8]Wang, H. H., Krstic, M., and Larsen, M., "Control of Deep-hysteresis Aeroengine Compressors," *Journal of Dynamic Systems Measurement and Control*, Vol. 122, No. 1, 2000, pp. 140–152.

[9]Liaw, D. C., and Huang, J. T., "Fuzzy Control for Stall Recovery in Compressor Dynamics," *Journal of Control Systems and Technology*, Vol. 6, No. 4, 1998, pp. 231–241.

[10]Moore, F. K., "A Theory of Rotating Stall of Multistage Axial Compressors: Part I—Small Disturbances," *Journal of Engineering for Gas Turbines and Power*, Vol. 106, 1984, pp. 313–320.

[11]Moore, F. K., and Greitzer, E. M., "A Theory of Post-stall Transient in Axial Compressors: Part I—Development of Equations," *Journal of Engineering for Gas Turbines and Power*, Vol. 108, Jan. 1986, pp. 68–76.

[12]Dowell, E. H., and Hall, K. C., "Eigenmode Analysis in Unsteady Aerodynamics: Reduced Order Models," *Applied Mechanics Review*, Vol. 50, No. 6, 1997, pp. 371–386.

[13]Leonard, B. P., "A Stable and Accurate Convective Modeling Procedure Based on Quadratic Upstream Interpolation," *Computer Methods in Applied Mechanics and Engeneering*, Vol. 19, No. 1, 1979, pp. 59–98.

[14]Fornberg, B., "Steady Incompressible Flow Past a Row of Circular Cylinders," *Journal of Fluid Mechanics*, Vol. 225, 1991, pp. 655–671.

[15]Adamson, T. C., Jr., and Messiter, A. F., "Analysis of Two-Dimensional Interactions Between Shock Waves and Boundary Layers," *Annual Review of Fluid Mechanics*, Vol. 12, 1980, pp. 103–138.